Atmospheric Environment 170 (2017) 108–117

Contents lists available at ScienceDirect

Atmospheric Environment

journal homepage: www.elsevier.com/locate/atmosenv

The influence of roadside solid and vegetation barriers on near-road air quality

Masoud Ghasemian*, Seyedmorteza Amini, Marko Princevac

Department of Mechanical Engineering, University of California, Riverside, CA 92521, USA

HIGHLIGHTS

- The Influence of roadside barriers on the near-road air quality was investigated.
- RANS technique coupled with the $k-\varepsilon$ realizable turbulence model was utilized.
- Vegetation barrier depending on LAD can improve or deteriorate the air quality.
- The dense canopy can improve the near-road air quality by inducing vertical mixing.

ARTICLE INFO

Article history:
Received 23 May 2017
Received in revised form
19 August 2017
Accepted 20 September 2017
Available online 21 September 2017

Keywords:
Air pollution
Solid barriers
Vegetation barriers
Computational fluid dynamics
Vehicle emission
$k-\varepsilon$ turbulence model

ABSTRACT

The current study evaluates the influence of roadside solid and vegetation barriers on the near-road air quality. Reynolds Averaged Navier-Stokes (RANS) technique coupled with the $k-\varepsilon$ realizable turbulence model is utilized to investigate the flow pattern and pollutant concentration. A scalar transport equation is solved for a tracer gas to represent the roadway pollutant emissions. In addition, a broad range of turbulent Schmidt numbers are tested to calibrate the scalar transport equation. Three main scenarios including flat terrain, solid barrier, and vegetative barrier are studied. To validate numerical methodology, predicted pollutant concentration is compared with published wind tunnel data. Results show that the solid barrier induces an updraft motion and lofts the vehicle emission plume. Therefore, the ground-level pollutant concentration decreases compared to the flat terrain. For the vegetation barrier, different sub-scenarios with different vegetation densities ranging from approximately flat terrain to nearly solid barrier are examined. Dense canopies act in a similar manner as a solid barrier and mitigate the pollutant concentration through vertical mixing. On the other hand, the high porosity vegetation barriers reduce the wind speed and lead to a higher pollutant concentration. As the vegetation density increases, i.e. the barrier porosity decreases, the recirculation zone behind the canopy becomes larger and moves toward the canopy. The dense plant canopy with $LAD = 3.33\ m^{-2}m^3$ can improve the near-road air quality by 10% and high porosity canopy with $LAD = 1\ m^{-2}m^3$ deteriorates near-road air quality by 15%. The results of this study can be implemented as green infrastructure design strategies by urban planners and forestry organizations.

Published by Elsevier Ltd.

1. Introduction

Exposure to traffic related air pollution leads to public health concerns such as respiratory problems, birth and developmental defects, premature mortality, cardiovascular effects and cancer for populations that live and work in the vicinity of major roadways (Crilley et al., 2017; Friberg et al., 2017; Goel and Kumar, 2016; Pu and Yang, 2014; Venkatram et al., 2013; Zauli Sajani et al., 2016). Therefore, it is critical to tackle these problems by near-road pollutant level mitigation. The near-road air quality can be improved directly by deploying vehicle emission control techniques, using alternative fuels or Electic Vehicles (EV), or via passive pollutant control and roadside configuration design such as solid and vegetative barriers. Passive barriers, in particular, offer other benefits such as noise reduction, shading, aesthetics and ecosystem service.

Several studies have evaluated the influence of solid barriers on near-road air quality (Amini et al., 2016; Baldauf et al., 2016; Hagler

* Corresponding author.
E-mail address: mghas002@ucr.edu (M. Ghasemian).

https://doi.org/10.1016/j.atmosenv.2017.09.028
1352-2310/Published by Elsevier Ltd.

et al., 2011; Pournazeri and Princevac, 2015; Schulte et al., 2014; Steffens et al., 2014, 2013). Solid barriers induce a significant vertical mixing and shift the plume upward through an induced updraft motion. Therefore, they can improve the air quality by increasing the initial plume dilution and plume height.

Vegetation barriers are inherently more complex compared to the solid barriers. Vegetation is a porous medium consisting of leaves and branches that are permeable to wind. Flow that passes through vegetation is different from flow around solid barriers. Wake extends further downstream and the recirculation zone is far from the vegetation barriers (Gromke, 2011). Finnigan (2000) and Raupach and Thom (1981) reviewed the turbulent flow structure within and around vegetation canopies. The air pollution removal capacity of plant canopies by deposition and filtration mechanisms have been focus of studies by Nowak et al. (2006) and Tallis et al. (2011). Several studies have been devoted to aerodynamics effects of tree canopies on local flow and pollutant concentration in street canyon configurations (Amorim et al., 2013; Buccolieri et al., 2011, 2009; Gromke, 2011; Gromke et al., 2016, 2008; Gromke and Blocken, 2015; Gromke and Ruck, 2012; Li et al., 2016; Pugh et al., 2012). The presence of trees in urban street canyon reduces the circulation, ventilation, and air exchange within canyon, and consequently increases the overall concentration level (Balczó et al., 2009; Salim et al., 2011; Vos et al., 2013; Wania et al., 2012).

Al-Dabbous and Kumar (2014) investigated the impact of roadside vegetation barriers on the airborne nanoparticles and roadside pedestrian's exposure under varying wind conditions. Their results showed that presence of vegetation barriers reduce particle number concentration by 37% during the cross-road winds. Jeanjean et al. (2015) employed CFD to evaluate the effectiveness of trees at dispersing road traffic emissions on a city scale. Their results showed that trees increase turbulence and wind velocity, consequently reducing ambient concentrations of road traffic emissions by 7% at pedestrian height on average. Steffens et al. (2012) explored the vegetation barriers effects on particle size distributions in a near-road environment. Although effects vary depending on particle size, they found that an increase in leaf area density (LAD) reduces particle concentration. In addition, increasing wind speed leads to particle impaction enhancement and particle diffusion reduction resulting in concentration reduction for particles greater than 50 nm but concentration increase for particles smaller than 50 nm. Hagler et al. (2012) measured roadside structural barrier and thin tree stand impact on near-road ultrafine particle concentrations. Their results showed that solid barrier lowered concentration by approximately 50% but there is no clear trend for vegetative barriers and in some cases, higher concentration is observed behind the vegetative barrier with respect to the flat terrain. However, they recommended other configurations of vegetative barriers, such as greater density and wider buffer. Field measurement by Lin et al. (2016) showed that vegetation barriers with full foliage reduced Ultrafine Particle and CO concentration by 37.7–63.6% and 23.6–56.1%, respectively. But there was no significant reduction in ultrafine particle concentration for the deciduous barrier during winter.

Pollutant concentration behind vegetative barriers can be mitigated by increase in particle deposition and vertical mixing, or it can be increased by windbreak effects behind the barrier, leading to a lower convective and turbulent transport in the barrier wake. Therefore, several studies have shown significant improvement in air quality behind roadside vegetation (Al-Dabbous and Kumar, 2014; Baldauf, 2017; Brantley et al., 2014; Steffens et al., 2012; Tong et al., 2016), while others (De Maerschalck et al., 2008; Hagler et al., 2012; Lin et al., 2016; Setälä et al., 2013) concluded that the roadside vegetation barriers have no effect or even potentially deteriorate near-road air quality. The vegetation density is the major difference among these two groups of studies. The former includes dense, wide, and full foliage canopies, while the latter consist of thin and deciduous canopies.

This study aims to answer this contradiction and provide a clear insight into the flow within and past canopies. To the author's knowledge, this is the first study that correlates the near-road pollutant concentration with the vegetation density. The current study utilizes Computational Fluid Dynamics (CFD) technique which can play a key role in improving our understanding of the influence of vegetation on the wind flow pattern and air pollutant concentration (Abhijith and Gokhale, 2015; Gromke and Blocken, 2015; Li et al., 2013; Xue and Li, 2017). Several Reynolds averaged Navier-Stokes simulations coupled with the $k-\varepsilon$ realizable turbulence model are performed to investigate the flow pattern behind the solid and vegetative barriers. Different vegetation densities ranging from approximately flat terrain to nearly solid barrier are examined to evaluate the correlation between pollutant concentration and vegetation density. This paper provides deeper insight into roadside vegetation design characteristics in order to implement them as an air pollution mitigation strategy. Ultimately, the outcome of this study can be exploited by urban planners, land managers and regulatory organizations to implement different green infrastructure design options.

2. Governing equations

The Reynolds Averaged Navier-Stokes (RANS) equations are employed to compute the flow and turbulence fields. Mass and momentum conservation equations for incompressible flow are defined as follows:

$$\frac{\partial u_j}{\partial x_j} = 0 \tag{1}$$

$$\rho u_j \frac{\partial u_i}{\partial x_j} = -\frac{\partial P}{\partial x_i} + (\mu + \mu_t)\frac{\partial}{\partial x_j}\left(\frac{\partial u_i}{\partial x_j} + \frac{\partial u_j}{\partial x_i}\right) \tag{2}$$

where u_i and u_j are the averaged velocity components in x_i and x_j directions, respectively, μ and μ_t are the dynamic and eddy viscosities, respectively and the $k-\varepsilon$ turbulence model has been employed to compute the turbulence field. This turbulence model solves two transport equations for turbulent kinetic energy, k, and turbulent dissipation rate, ε (Wilson, 1985). The $k-\varepsilon$ turbulence model includes different variations such as standard $k-\varepsilon$, Renormalization Group (RNG) $k-\varepsilon$, and realizable $k-\varepsilon$. All variations have similar transport equations for turbulent kinetic energy and turbulent dissipation rate but they have different turbulent viscosity calculation methods, generation and destruction terms in the ε equation, and different turbulent Prandtl numbers that govern the diffusion of k and ε. Numerical simulation of dispersion around an isolated cubic building conducted by Tominaga and Stathopoulos (2009) showed that the standard $k-\varepsilon$ turbulence model provides inadequate results for the concentration field compared to the RNG and realizable $k-\varepsilon$ turbulence models. Numerical simulation of windbreak aerodynamics conducted by Bourdin and Wilson (2008) suggested that realizable $k-\varepsilon$ turbulence model is the optimal turbulence model to capture the windbreak aerodynamics. Therefore, this study utilizes the realizable $k-\varepsilon$ turbulence model to compute turbulent viscosity.

The vegetation exerts a drag force on the air flow. This flow obstruction can be represented by sink terms in the streamwise and vertical directions in the momentum equation.

$$S_x = -\rho C_d LADuU \tag{3}$$

$$S_z = -\rho C_d LADwU \tag{4}$$

where ρ is air density, C_d is the bulk drag coefficient which depends on tree type and its density, and *LAD* is the leaf area density defined as the ratio of leaf surface area to the total volume occupied by vegetation. The *LAD* depends on the type of tree and varies with height over the tree crown. *LAD* typically varies between 0.5 and 2 m^2m^{-3} (Gromke and Blocken, 2015). The streamwise and vertical velocity components are denoted by u and w, respectively and U is the velocity magnitude.

The wind permeability of vegetation canopy depends on the pore volume fraction and pore orientation to the flow. Pressure loss coefficient, λ, is a good measure for the permeability of vegetation canopy. The pressure loss coefficient in the forced convection flows is defined according to:

$$\lambda = \frac{\Delta p_{st}}{\frac{1}{2}\rho u^2 d} \tag{5}$$

where Δp_{st} is the static pressure drop over the porous media and d is streamwise thickness. Pressure loss coefficient of vegetation shelterbelts formed by broad-leaved trees measured in forced convective flows by Grunert et al. (1984) are provided in Fig. 1(reproduced from tabular values summarized in Gromke (2012)). In this figure, density ρ_s quantifies the branch arrangement in the shelterbelt. Unit value of ρ_s refers to the typical branch arrangement and cases with dense ($\rho_s = 1.33$) and less dense ($\rho_s = 0.67$) branch arrangements are investigated.

According to Fig. 1, pressure loss coefficient varies substantially from less than 1 to over 14. To address most of the vegetation shelterbelts in this study we adopted $\lambda = 2\ m^{-1}$. Raupach et al. (2001) proposed following relationship between bulk drag coefficient and screen pressure coefficient, λ:

$$C_d = \frac{\Gamma_{b1}\lambda}{\lambda + \Gamma_{b1}\lambda_1} \tag{6}$$

where Γ_{b1} is the bulk drag coefficient for a solid fence here taken as $\Gamma_{b1} = 1.07$ according to Jacobs (1983) and, $\lambda_1 = 1.5$ is the empirical constant. Introducing $\lambda = 2\ m^{-1}$ in equation (6) results in $C_d = 0.6$.

As air moves through the vegetation barriers, leaves and branches disturb the mean flow and convert kinetic energy to turbulent kinetic energy. The generated turbulence has small eddy scales; therefore, it dissipates rapidly. The impact of canopy on turbulence field can be represented as follows:

$$S_k = -\rho C_d LAD\left(\beta_p u^3 - \beta_d uk\right) \tag{7}$$

$$S_\varepsilon = -\rho C_d LAD\left(C_{\varepsilon 4}\beta_p \frac{\varepsilon}{k} u^3 - C_{\varepsilon 5}\beta_d u\varepsilon\right) \tag{8}$$

where S_k represents the turbulence generation due to vegetation elements, S_ε expresses the rapid dissipation of turbulent kinetic energy, β_p is the fraction of the mean flow kinetic energy converted to turbulent kinetic energy, and β_d is the fraction of turbulent kinetic energy dissipated within the canopy. The different parameters and coefficients in the vegetation model were listed in Table 1.

An additional advection-diffusion equation is solved for a passive tracer gas to represent the road traffic emissions:

Table 1
Parameters and coefficients in the vegetation model (Gromke and Blocken, 2015).

β_d	β_p	$C_{\varepsilon 4}$	$C_{\varepsilon 4}$
5.1	1	0.9	0.9

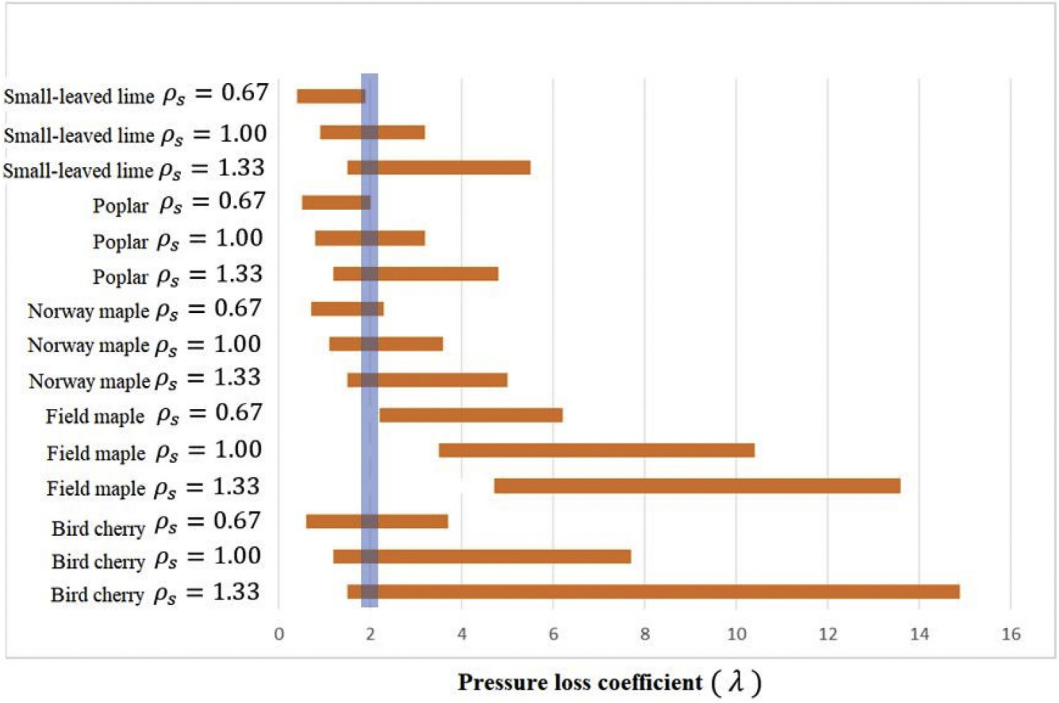

Fig. 1. Pressure loss coefficient for leaved vegetation shelterbelt measured by Grunert et al. (1984) (adapted from Gromke (2012)).

$$\frac{\partial}{\partial x_j}(u_j\varphi) = \frac{\partial}{\partial x_j}\left(\left(D_\varphi + \frac{\mu_t}{\rho Sc_t}\right)\frac{\partial}{\partial x_j}\varphi\right) \quad (9)$$

where φ is the pollutant concentration, D_φ is the molecular diffusion coefficient and Sc_t is the turbulent Schmidt number. The turbulent Schmidt number varies for different configurations and it should be determined according to the local flow characteristics and dominant flow structures.

Richards and Hoxey (1993) vertical profiles are utilized to specify the mean velocity, turbulent kinetic energy and dissipation rate variations at the inlet boundary condition for the neutral stratification:

$$U(z) = \frac{u_*}{\kappa} ln\frac{z+z_0}{z_0} \quad (10)$$

$$k = \frac{u_*^2}{\sqrt{C_\mu}} \quad (11)$$

$$\varepsilon = \frac{u_*^3}{\kappa(z+z_0)} \quad (12)$$

where $U(z)$ is the wind speed at height of z above the ground, u_* is the friction velocity extracted from the logarithmic profile with the wind speed value at the reference height, κ is the von Karman's constant (0.41), z_0 is ground roughness length and C_μ is a coefficient used to define the eddy viscosity in $k-\varepsilon$ turbulence model.

3. Problem description

In this study, three main scenarios are studied: 1) flat terrain, 2) solid barrier with height of $1.5H$ and thickness of 0.5 m ($H = 6m$), and 3) vegetation barrier with height of $1.5H$ and thickness of $1.5H$. To evaluate the influence of vegetation porosity, five different *LAD* were investigated. These include *LAD* = 0.17, 0.42, 1, 1.25 and 3.33 $m^{-2}m^3$. A summary of different scenarios is listed in Table 2. Two line sources located at $x = \pm 1.65H$ replicate the roadway emissions and the origin is located at the middle of the line sources. The line sources emit ethane as tracer gas. The solid barrier is located at $x = 3H$ and the vegetation barrier starts at $x = 3H$ and is extended to $x = 4.5H$. Fig. 2 depicts a schematic of different scenarios. The wind speed is 2.98 m/s at height of 30 m and wind direction is perpendicular to the road. The utilized logarithmic boundary layer has a roughness length of $z_0 = 0.27$ m and a friction velocity of $u_* = 0.25$ m/s.

3.1. Numerical method

A two-dimensional incompressible steady computational fluid dynamic solver is employed to solve the Navier–Stokes equations using RANS technique. Due to the incompressibility of the flow, the pressure-based solver is chosen, which is traditionally implemented to solve low-speed incompressible flows. The SIMPLE (Semi-Implicit Method for Pressure-Linked Equations) algorithm (Patankar, 1980) is chosen for coupling the velocity–pressure equations. Spatial discretization has been carried out using a least squares cell based algorithm for gradients, the second order upwind scheme for momentum, turbulent kinetic energy and turbulent dissipation rate and concentration. The residual target is that the normalized RMS (root mean square) errors for each conservation balance over the entire mesh reach to less than 10^{-5}.

A structured non-uniform grid is employed to discretize the computational domain. A schematic of computational grid for solid barrier scenario is shown in Fig. 3. The dimensions of computational domain in streamwise and vertical directions are 300 m and 100 m, respectively. The grid points are clustered near the ground, barrier and pollutant sources, where the velocity and concentration gradients are larger. The first grid close to the ground has a height of 0.25 m and it grows with an expansion ratio of 1.2. The grid refinement study showed that the computational grid with 18,000 cells leads to the required grid resolution.

In order to compare our results with wind tunnel data (Heist et al., 2009), concentration is reported in normalized form $\chi = \frac{\varphi U_r L_x L_y}{Q}$, where φ is the concentration, U_r is the wind speed at reference height, Q is the pollutant emission rate, L_x and L_y are the dimensions of source section in streamwise and crosswise directions, respectively.

3.2. Turbulent Schmidt number calibration and numerical method validation

The turbulent Schmidt number is the ratio of turbulent (eddy) viscosity to turbulent mass diffusivity:

$$Sc_t = \frac{\mu_t}{\rho D_t} \quad (13)$$

The turbulent Schmidt number differs for different configurations and it should be determined according to the local flow characteristics and dominant flow structures (Flesch et al., 2002; Riddle et al., 2004; Thaker and Gokhale, 2015; Tominaga and Stathopoulos, 2013). Tominaga and Stathopoulos (2007) reported that the optimum turbulent Schmidt numbers for atmospheric dispersion are widely distributed in the range of 0.2–1.3.

In order to determine the optimum value for turbulent Schmidt number, three different turbulent Schmidt numbers $Sc_t = 0.4$, 0.7 and 1 were examined. Fig. 4 shows the vertical normalized pollutant concentration distribution behind $1H$ high solid barrier at $x/H = 7$ for different turbulent Schmidt numbers and results are compared with wind tunnel data (Heist et al., 2009). At the lower turbulent Schmidt numbers, there is higher pollutant dispersion which causes decrease in ground level concentration and increase in elevated level concentration. The comparison of results with

Table 2
Different simulation scenarios.

Case	Barrier type	Barrier height ($H = 6$ m)	Barrier thickness	Drag coefficient (C_d)	LAD ($m^{-2}m^{-3}$)	Wind speed [a] ($m\ s^{-1}$)
A	No barrier	–	–	–	–	2.98
B	Solid	$1.5H$	0.5 [m]	–	–	2.98
C	Vegetative	$1.5H$	$1.5H$	0.6	1	2.98
D	Vegetative	$1.5H$	$1.5H$	0.6	0.17	2.98
E	Vegetative	$1.5H$	$1.5H$	0.6	0.42	2.98
F	Vegetative	$1.5H$	$1.5H$	0.6	1.25	2.98
G	Vegetative	$1.5H$	$1.5H$	0.6	3.33	2.98

[a] Wind speed at height of 30 m.

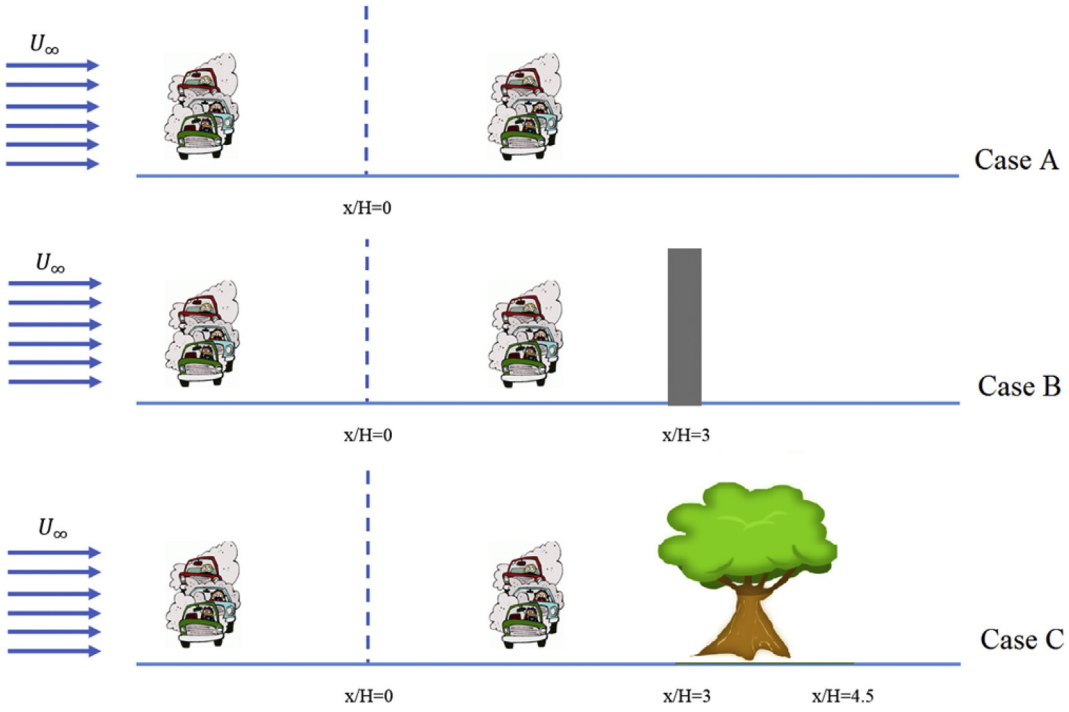

Fig. 2. Different scenarios; (case A): flat terrain, (case B): solid barrier, (Case C): vegetation barrier.

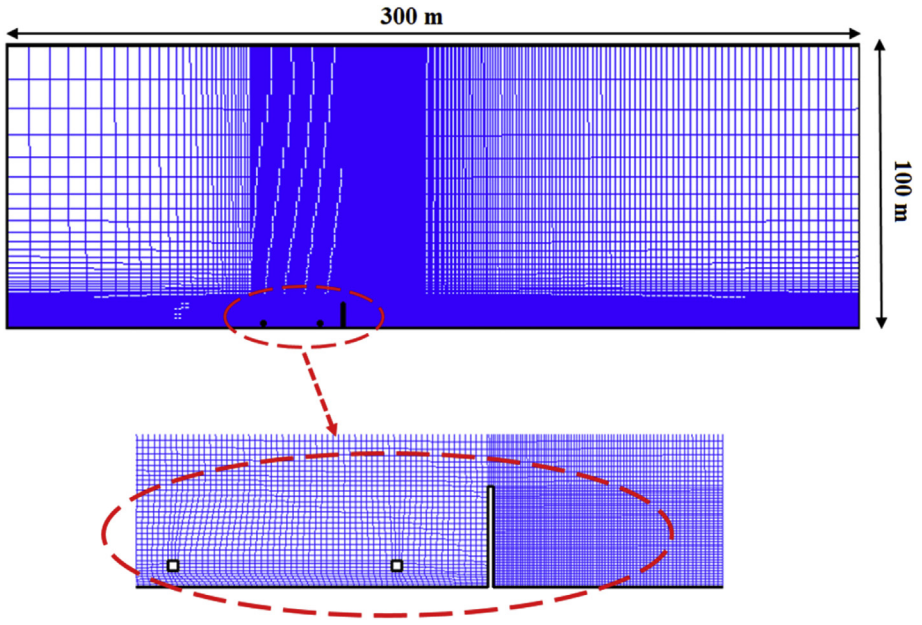

Fig. 3. Structured computational grid.

wind tunnel data shows that using $Sc_t = 0.4$ and $Sc_t = 1$ under-predicted and over-predicted the ground-level pollutant concentration, respectively. These under-prediction and over-prediction in pollutant concentration can be interpreted by physical meaning and definition of turbulent Schmidt number. Based on equation (13), lower turbulent Schmidt number ($Sc_t = 0.4$) means higher turbulent mass diffusivity and pollutant dispersion, consequently resulting in lower pollutant concentration close to the pollutant source. Therefore, $Sc_t = 0.4$ under-predicts the ground level concentration. The pollutant concentration demonstrates a good agreement with experimental data at $Sc_t = 0.7$. Therefore, this turbulent Schmidt number is chosen as the optimal value.

4. Results and discussion

4.1. Streamlines and pollutant concentration

Fig. 5 depicts the contour of velocity and streamlines for flat terrain (case A), solid barrier (case B), and vegetation barrier (case C). For the flat terrain, the streamlines are mostly horizontal. The

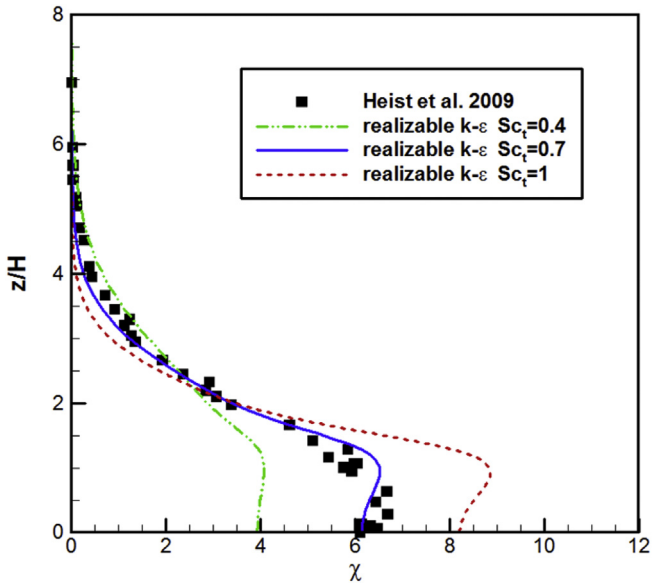

Fig. 4. Vertical distribution of concentration behind $1H$ high solid barrier at $x/H = 7$ for different turbulent Schmidt numbers and wind tunnel data measured by Heist et al. (2009) (adapted from Hagler et al. (2011)).

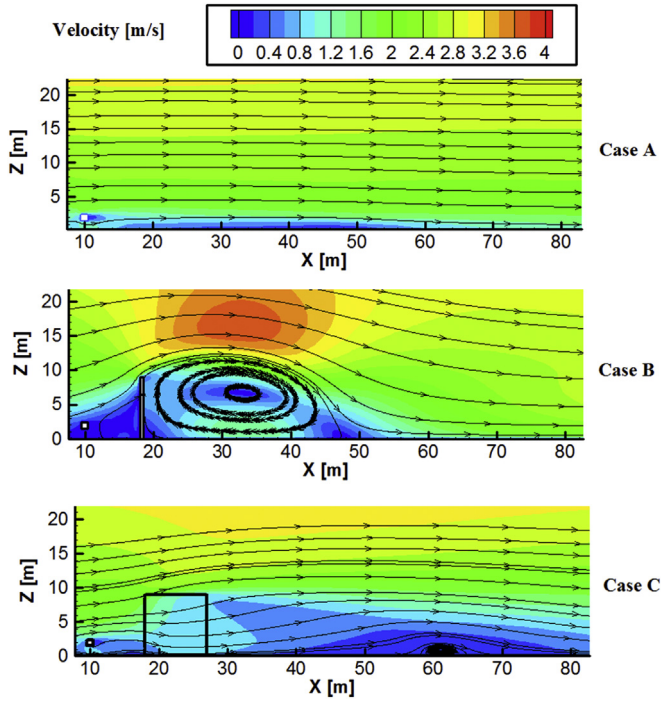

Fig. 5. Contour of velocity and streamlines; (case A): flat terrain, (case B): solid barrier, (case C): vegetation barrier.

solid barrier induces a significant vertical velocity component and deflects the streamlines. Moreover, there is a recirculation zone behind the solid barrier. On the other hand, the vegetation barrier creates a low wind speed region downstream. But similar to the solid barrier, a recirculation zone forms behind the vegetation barrier. However, due to the existence of the mean flow through the vegetation barrier, this recalculation is advected far downstream and it is not strong enough to induce an updraft motion and to raise the plume.

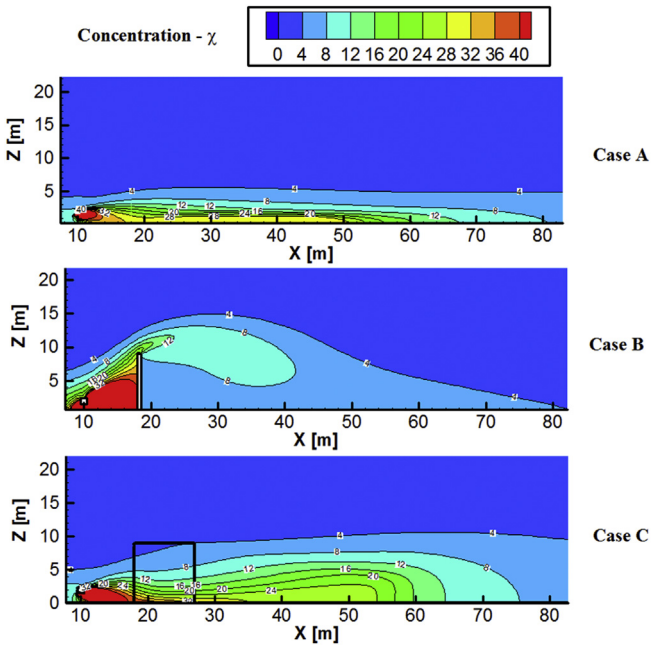

Fig. 6. Contour of pollutant concentration; (case A): flat terrain, (case B): solid barrier, (case C): vegetation barrier.

Fig. 6 shows the contour of pollutant concentration for different scenarios, flat terrain (case A), solid barrier (case B), and vegetation barrier (case C). The solid barrier induces an updraft motion which causes plume lofting and increases the pollutant dispersion. Therefore, solid barrier improves the air quality behind the barrier by effectively converting ground level source into an elevated source. On the other hand, the vegetation barrier reduces the wind speed which results in slower dispersion of the pollutant within or behind the canopy. It does not induce an updraft motion to raise the plume from the ground. Therefore, the presented case of the vegetation barrier increases the pollutant concentration. The pollutant concentration was averaged in the region $0 < y < 3$ m and $27\ m < x < 127\ m$ ($x = 27$ m is the end of vegetation barrier, and the gradient of concentration becomes negligible after $x = 127$ m). The averaged pollutant concentration in this region shows that the solid barrier improved the near-road air quality by 58% and vegetation barrier deteriorated the air quality by 15% with respect to the flat terrain. We examine the effects of different vegetation porosities in the next section.

4.2. Vegetation density effects on the flow pattern and pollutant concentration

In this section, the change of flow pattern and pollutant concentration with vegetation density are analyzed. Different leaf area densities ranging from approximately undisturbed flat terrain to nearly solid barrier are examined. A summary of these scenarios has been provided in Table 2 (cases C-G). The leaf area density varies in the range of 0.17–3.33 m^2m^{-3}. Fig. 7 shows contours of velocity and streamlines for cases C-G with different leaf area densities $LAD = 0.17$, 0.42, 1, 1.25, and 3.33 m^2m^{-3}. For cases D and E with leaf area density of $LAD = 0.17\ m^2m^{-3}$ and $0.42\ m^2m^{-3}$, there is no obvious change in the streamlines and the flow pattern approximately represents a flat terrain. As the vegetation density and leaf area density increases, the reduction in wind speed increases. For cases C and F with leaf area density of $LAD = 1\ m^2m^{-3}$ and $LAD = 1.25\ m^2m^{-3}$, there are two distinct zones behind the

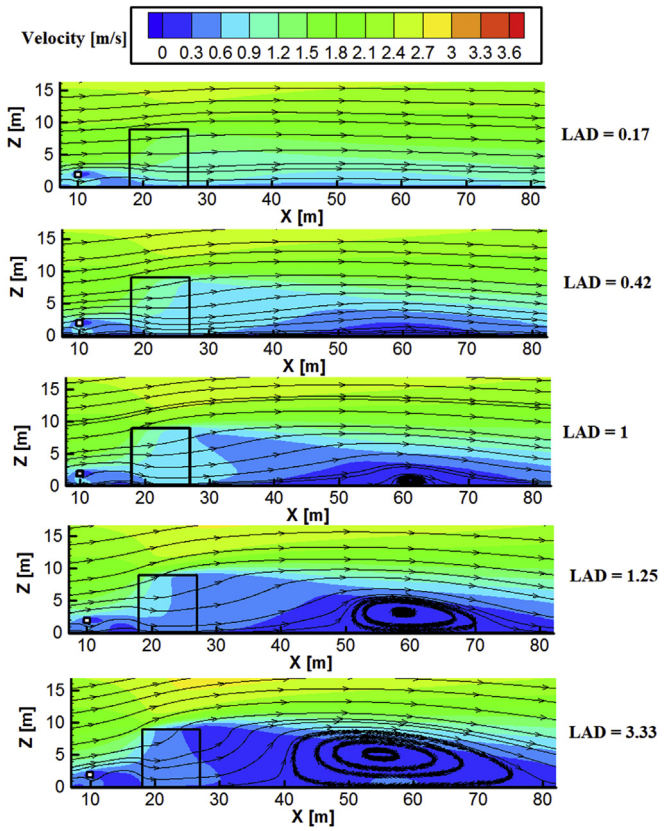

Fig. 7. Contour of velocity magnitude and streamlines for different leaf area densities: Case D ($LAD = 0.17\ m^2m^{-3}$) - Case E ($LAD = 0.42\ m^2m^{-3}$) - Case C ($LAD = 1.00\ m^2m^{-3}$) - Case F ($LAD = 1.25\ m^2m^{-3}$) - Case G ($LAD = 3.33\ m^2m^{-3}$).

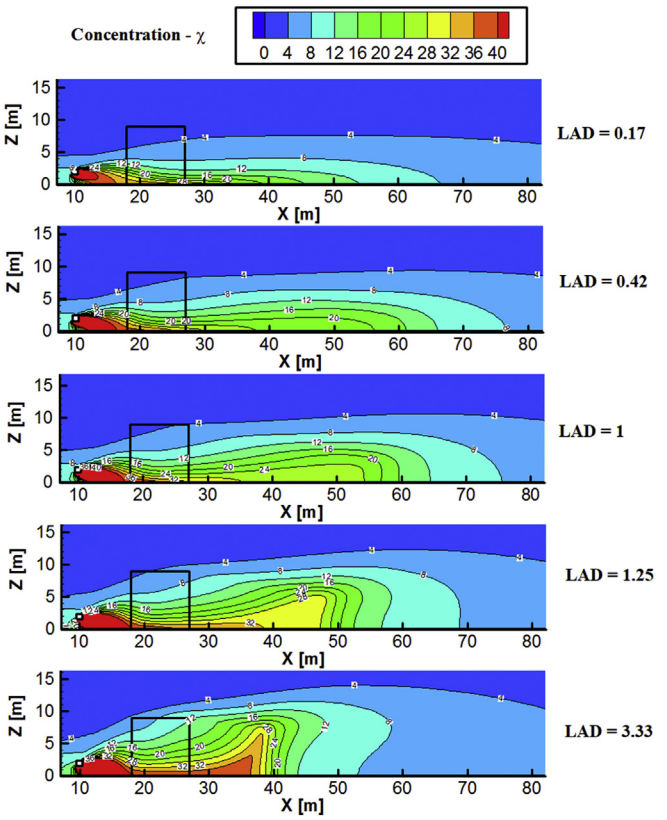

Fig. 8. Contour of pollutant concentration for different leaf area densities: Case D ($LAD = 0.17\ m^2m^{-3}$) - Case E ($LAD = 0.42\ m^2m^{-3}$) - Case C ($LAD = 1.00\ m^2m^{-3}$) - Case F ($LAD = 1.25\ m^2m^{-3}$) – Case G ($LAD = 3.33\ m^2m^{-3}$).

vegetative barrier, a quiet zone immediately behind the vegetative barriers characterized by reduced turbulence and smaller eddy size. Further downwind lies a small and weak recirculation zone with increased turbulence. For case G with leaf area density of $LAD = 3.33\ m^2m^{-3}$, vegetative barrier acts as a solid obstacle that deflects the wind upward and compresses the flow streamlines over the top. The flow is lofted over the canopy and the recirculation zone is observed immediately downwind. As the leaf area density increases, the center of recirculation zone moves upward and towards the vegetative barrier. Also, the separation point moves toward the vegetative barrier, but the reattachment point remains roughly constant. Consequently, the size and strength of recirculation zone increases.

Fig. 8 depicts the contour of pollutant concentration behind the vegetative barriers with different leaf area densities $LAD = 0.17,\ 0.42,\ 1,\ 1.25$, and $3.33\ m^2m^{-3}$. Initially, by increasing the leaf area density, the pollutant concentration behind the canopy increases. But as the leaf area density increases further, the pollutant concentration eventually decreases. The recirculation zone keeps the pollutant close to the barriers, resulting in decreased pollutant concentration away from the barrier for dense canopies (case G). The high LAD vegetation (case G) mixes the pollutant vertically by inducing recirculation mixing. Therefore, the concentration is more uniform with height compared to the low LAD vegetations (cases D and E). For the low leaf area density canopy (case D), the pollutant concentration contour is similar to the flat terrain while for the high leaf area density canopy the concentration is approaching that of the solid barrier.

Fig. 9 depicts the vertical distribution of normalized pollutant concentration for different canopy densities and a no-barrier scenario, at different distances from the roadway ($x/H = 7,\ 10,\ 15,$ and 20). As the vegetation density increases, the canopy induces more plume lofting. Therefore, the concentration profile is flatter for higher density canopies. At $x/H = 7$, the ground level concentration increases initially by leaf area density and it reaches to its maximum value at $LAD = 1.25\ m^2m^{-3}$. Further increasing the leaf area density leads to ground level concentration reduction. For instance, the normalized ground level concentration reduced to $\chi = 15$ for canopy with leaf area density of $LAD = 3.33\ m^2m^{-3}$ while it was $\chi = 32$ for $LAD = 1.25\ m^2m^{-3}$. At $x/H = 10$, $x/H = 15$ and $x/H = 20$, the ground level concentration has the same trend, but it reaches to its maximum value at $LAD = 0.42\ m^2m^{-3}$.

As mentioned earlier, there is no study that provides a quantitative correlation between the concentration and the vegetation porosity/density. In order to correlate the pollutant concentration and LAD, the pollutant concentration behind the canopy was averaged in the region $0 < y < 3\ m$ and $27\ m < x < 127\ m$ and then the averaged value was normalized with the flat terrain concentration. Fig. 10 depicts the variation of averaged concentration for different leaf area densities. The averaged concentration behind the canopy is initially increasing with the LAD before it starts to decrease. Due to larger penetration of pollutants and the windbreak effect, the canopies with high porosity deteriorate air quality behind them. On the other hand, vegetative barriers with higher densities mitigate the air pollution behind them. Generally, in canopies with high porosity, the windbreak effects (i.e. low wind region) are more dominant compared to the vertical mixing (i.e. recirculation).

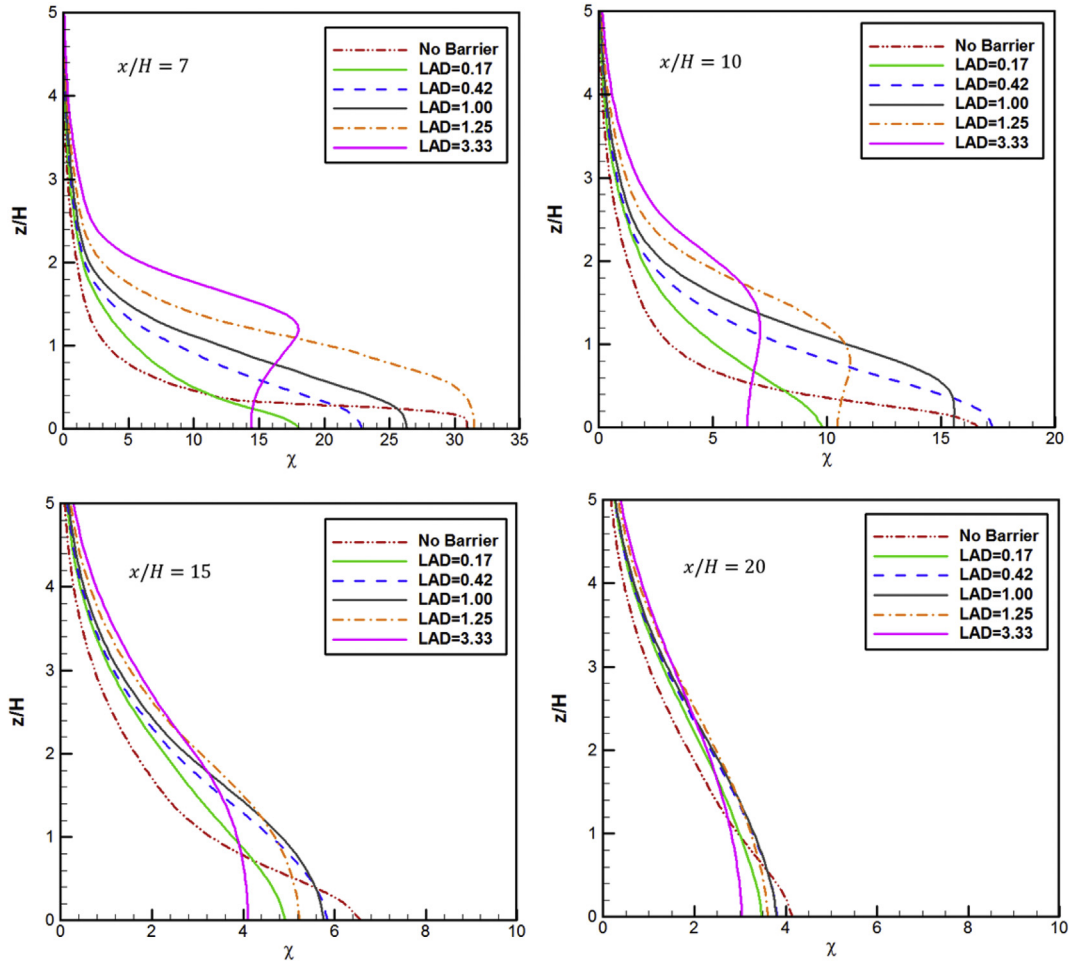

Fig. 9. Vertical distribution of normalized pollutant concentration at different distances from roadway ($x/H = 7$, $x/H = 10$, $x/H = 15$, $x/H = 20$) for different LAD and no-barrier scenario.

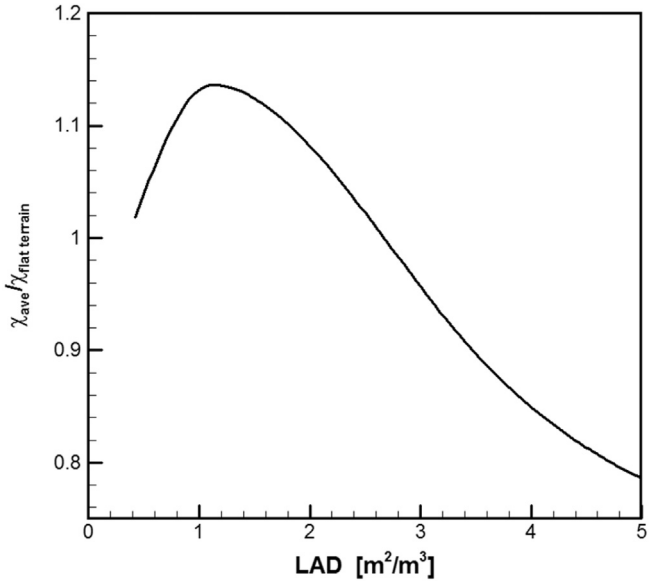

Fig. 10. Averaged pollutant concentration behind the vegetative barrier for different LAD.

5. Conclusion

Several computational fluid dynamic simulations were carried out to evaluate the influence of solid and vegetative barriers on the flow pattern and near-road air quality. Three main scenarios including flat terrain, solid barrier, and vegetative barrier were studied. Also, five sub-scenarios with different canopy densities were examined. The main conclusions can be summarized as follows:

- The turbulent Schmidt number calibration showed that $Sc_t = 0.7$ is the optimal value. $Sc_t = 0.4$ and $Sc_t = 1$ underpredicted and overpredicted the ground-level pollutant concentration, respectively.
- The solid barrier induces a vertical mixing and upward motion. This plume lofting decreases the ground-level pollutant concentration and improves the near-road air quality.
- As the vegetation density increases, the recirculation zone behind the canopy becomes stronger and moves toward the canopy.
- The dense canopies act in a similar manner as solid barrier and mitigate the pollutant concentration through vertical mixing and upwind deflection of the plume. For the modeled dense canopy with $LAD = 3.33\ m^{-2}m^3$, the near-road air quality was improved by 10% with respect to flat terrain. The solid barrier with the same height improved the air quality by 58%.

- The high porosity canopies reduce the wind speed and stagnate the pollutant within or behind the canopy. For vegetative barrier with $LAD = 1\ m^{-2}m^3$, the near-road air quality deteriorated by 15% with respect to the flat terrain.
- The examination of a wide range of vegetation density clarified that vegetations with low LAD deteriorates the near-road air quality, while dense canopies improve the air quality.
- The outcome of the current study can be deployed for green infrastructure design strategies in the urban planning and roadway configuration design.

References

Abhijith, K.V., Gokhale, S., 2015. Passive control potentials of trees and on-street parked cars in reduction of air pollution exposure in urban street canyons. Environ. Pollut. 204, 99–108. https://doi.org/10.1016/j.envpol.2015.04.013.

Al-Dabbous, A.N., Kumar, P., 2014. The influence of roadside vegetation barriers on airborne nanoparticles and pedestrians exposure under varying wind conditions. Atmos. Environ. 90, 113–124. https://doi.org/10.1016/j.atmosenv.2014.03.040.

Amini, S., Ahangar, F.E., Schulte, N., Venkatram, A., 2016. Using models to interpret the impact of roadside barriers on near-road air quality. Atmos. Environ. 138, 55–64. https://doi.org/10.1016/j.atmosenv.2016.05.001.

Amorim, J.H., Rodrigues, V., Tavares, R., Valente, J., Borrego, C., 2013. CFD modelling of the aerodynamic effect of trees on urban air pollution dispersion. Sci. Total Environ. 461–462, 541–551. https://doi.org/10.1016/j.scitotenv.2013.05.031.

Balczó, M., Gromke, C., Ruck, B., 2009. Numerical modeling of flow and pollutant dispersion in street canyons with tree planting. Meteorol. Z. 18, 197–206.

Baldauf, R., 2017. Roadside vegetation design characteristics that can improve local, near-road air quality. Transp. Res. Part D. Transp. Environ. 52, 354–361. https://doi.org/10.1016/j.trd.2017.03.013.

Baldauf, R.W., Isakov, V., Deshmukh, P., Venkatram, A., Yang, B., Zhang, K.M., 2016. Influence of solid noise barriers on near-road and on-road air quality. Atmos. Environ. 129, 265–276. https://doi.org/10.1016/j.atmosenv.2016.01.025.

Bourdin, P., Wilson, J.D., 2008. Windbreak Aerodynamics: is computational fluid dynamics Reliable. Boundary-Layer Meteorol. 181–208. https://doi.org/10.1007/s10546-007-9229-y.

Brantley, H.L., Hagler, G.S.W.J., Deshmukh, P., Baldauf, R.W., 2014. Field assessment of the effects of roadside vegetation on near-road black carbon and particulate matter. Sci. Total Environ. 468–469, 120–129. https://doi.org/10.1016/j.scitotenv.2013.08.001.

Buccolieri, R., Gromke, C., Di Sabatino, S., Ruck, B., 2009. Aerodynamic effects of trees on pollutant concentration in street canyons. Sci. Total Environ. 407, 5247–5256. https://doi.org/10.1016/j.scitotenv.2009.06.016.

Buccolieri, R., Salim, S.M., Leo, L.S., Di Sabatino, S., Chan, A., Ielpo, P., de Gennaro, G., Gromke, C., 2011. Analysis of local scale tree-atmosphere interaction on pollutant concentration in idealized street canyons and application to a real urban junction. Atmos. Environ. 45, 1702–1713. https://doi.org/10.1016/j.atmosenv.2010.12.058.

Crilley, L.R., Lucarelli, F., Bloss, W.J., Harrison, R.M., Beddows, D.C., Calzolai, G., Nava, S., Valli, G., Bernardoni, V., Vecchi, R., 2017. Source apportionment of fine and coarse particles at a roadside and urban background site in London during the 2012 summer ClearfLo campaign. Environ. Pollut. 220, 766–778. https://doi.org/10.1016/j.envpol.2016.06.002.

De Maerschalck, B., Janssen, S., Vankerkom, J., Mensink, C., van den Burg, A., Fortuin, P., 2008. CFD simulations of the impact of a line vegetation element along a motorway on local air quality. Hrvat. Meteoroloski Cas. 43 (PART 1), 339–344.

Finnigan, J., 2000. Turbulence in plant canopies. Annu. Rev. Fluid Mech. 32, 519–571.

Flesch, T.K., Prueger, J.H., Hatfield, J.L., 2002. Turbulent Schmidt number from a tracer experiment. Agric. For. Meteorol 111, 299–307. https://doi.org/10.1016/S0168-1923(02)00025-4.

Friberg, M.D., Kahn, R.A., Holmes, H.A., Chang, H.H., Ebelt, S., Tolbert, P.E., Russell, A.G., Mulholland, J.A., 2017. Daily ambient air pollution metrics for fi ve cities: evaluation of data- fusion-based estimates and uncertainties. Atmos. Environ. 158, 36–50. https://doi.org/10.1016/j.atmosenv.2017.03.022.

Goel, A., Kumar, P., 2016. Vertical and horizontal variability in airborne nanoparticles and their exposure around signalised traffic intersections. Environ. Pollut. 214, 54–69. https://doi.org/10.1016/j.envpol.2016.03.033.

Gromke, C., 2012. Modeling vegetation in Wind Engineering wind tunnel studies. Seventh Int. Colloq. Bluff Body Aerodyn. Appl. 1421–1428.

Gromke, C., 2011. A vegetation modeling concept for building and environmental aerodynamics wind tunnel tests and its application in pollutant dispersion studies. Environ. Pollut. 159, 2094–2099. https://doi.org/10.1016/j.envpol.2010.11.012.

Gromke, C., Blocken, B., 2015. Influence of avenue-trees on air quality at the urban neighborhood scale. Part I: quality assurance studies and turbulent Schmidt number analysis for RANS CFD simulations. Environ. Pollut. 196, 214–223. https://doi.org/10.1016/j.envpol.2014.10.016.

Gromke, C., Buccolieri, R., Di Sabatino, S., Ruck, B., 2008. Dispersion study in a street canyon with tree planting by means of wind tunnel and numerical investigations - evaluation of CFD data with experimental data. Atmos. Environ. 42, 8640–8650. https://doi.org/10.1016/j.atmosenv.2008.08.019.

Gromke, C., Jamarkattel, N., Ruck, B., 2016. Influence of roadside hedgerows on air quality in urban street canyons. Atmos. Environ. 139, 75–86. https://doi.org/10.1016/j.atmosenv.2016.05.014.

Gromke, C., Ruck, B., 2012. Pollutant concentrations in street canyons of different aspect ratio with avenues of trees for various wind directions. Boundary-Layer Meteorol. 144, 41–64. https://doi.org/10.1007/s10546-012-9703-z.

Grunert, F., Benndorf, D., Klingbeil, K., 1984. Neuere Ergebnisse zum Aufbau von Schutzpflanzungen. Beiträge für Forstwiss 18, 108–115.

Hagler, G.S.W., Lin, M.Y., Khlystov, A., Baldauf, R.W., Isakov, V., Faircloth, J., Jackson, L.E., 2012. Field investigation of roadside vegetative and structural barrier impact on near-road ultrafine particle concentrations under a variety of wind conditions. Sci. Total Environ. 419, 7–15. https://doi.org/10.1016/j.scitotenv.2011.12.002.

Hagler, G.S.W., Tang, W., Freeman, M.J., Heist, D.K., Perry, S.G., Vette, A.F., 2011. Model evaluation of roadside barrier impact on near-road air pollution. Atmos. Environ. 45, 2522–2530. https://doi.org/10.1016/j.atmosenv.2011.02.030.

Heist, D.K., Perry, S.G., Brixey, L.A., 2009. A wind tunnel study of the effect of roadway configurations on the dispersion of traffic-related pollution. Atmos. Environ. 43, 5101–5111. https://doi.org/10.1016/j.atmosenv.2009.06.034.

Jacobs, A.F.G., 1983. Flow Arounda Line Obstacle. Wageningen Agricultural University, Wageningen, The Netherlands.

Jeanjean, A.P.R., Hinchliffe, G., McMullan, W.A., Monks, P.S., Leigh, R.J., 2015. A CFD study on the effectiveness of trees to disperse road traffic emissions at a city scale. Atmos. Environ. 120, 1–14. https://doi.org/10.1016/j.atmosenv.2015.08.003.

Li, J.F., Zhan, J.M., Li, Y.S., Wai, O.W.H., 2013. CO2 absorption/emission and aerodynamic effects of trees on the concentrations in a street canyon in Guangzhou, China. Environ. Pollut. 177, 4–12. https://doi.org/10.1016/j.envpol.2013.01.016.

Li, X.B., Lu, Q.C., Lu, S.J., He, H. Di, Peng, Z.R., Gao, Y., Wang, Z.Y., 2016. The impacts of roadside vegetation barriers on the dispersion of gaseous traffic pollution in urban street canyons. Urban For. Urban Green 17, 80–91. https://doi.org/10.1016/j.ufug.2016.03.006.

Lin, M.Y., Hagler, G., Baldauf, R., Isakov, V., Lin, H.Y., Khlystov, A., 2016. The effects of vegetation barriers on near-road ultrafine particle number and carbon monoxide concentrations. Sci. Total Environ. 553, 372–379. https://doi.org/10.1016/j.scitotenv.2016.02.035.

Nowak, D.J., Crane, D.E., Stevens, J.C., 2006. Air pollution removal by urban trees and shrubs in the United States. Urban For. Urban Green 4, 115–123. https://doi.org/10.1016/j.ufug.2006.01.007.

Patankar, S.V., 1980. Numerical Heat Transfer and Fluid Flow. McGraw-Hill.

Pournazeri, S., Princevac, M., 2015. Sound wall barriers: near roadway dispersion under neutrally stratified boundary layer. Transp. Res. Part D. Transp. Environ. 41, 386–400. https://doi.org/10.1016/j.trd.2015.09.025.

Pu, Y., Yang, C., 2014. Estimating urban roadside emissions with an atmospheric dispersion model based on in-field measurements. Environ. Pollut. 192, 300–307. https://doi.org/10.1016/j.envpol.2014.05.019.

Pugh, T.M., Mackenzie, R.A., Whyatt, D.J., Hewitt, N.C., 2012. Effectiveness of green infrastructure for improvement of air quality in urban street canyons. Environ. Sci. Technol. 46, 7692–7699. https://doi.org/10.1021/es300826w.

Raupach, M.R., Thom, A.S., 1981. Turbulence in and above plant canopies. Annu. Rev. Fluid Mech. 13, 97–129. https://doi.org/10.1146/annurev.fl.13.010181.000525.

Raupach, M.R., Woods, N., Dorr, G., Leys, J.F., Cleugh, H.A., 2001. The entrapment of particles by windbreaks. Atmos. Environ. 35, 3373–3383. https://doi.org/10.1016/S1352-2310(01)00139-X.

Richards, P., Hoxey, R., 1993. Appropriate boundary conditions for computational wind engineering models using the k–e turbulence mode. J. Wind Eng. Ind. Aerodyn. 46–47, 145–153.

Riddle, A., Carruthers, D., Sharpe, A., McHugh, C., Stocker, J., 2004. Comparisons between FLUENT and ADMS for atmospheric dispersion modelling. Atmos. Environ. 38, 1029–1038. https://doi.org/10.1016/j.atmosenv.2003.10.052.

Salim, S.M., Cheah, S.C., Chan, A., 2011. Numerical simulation of dispersion in urban street canyons with avenue-like tree plantings: comparison between RANS and LES. Build. Environ. 46, 1735–1746. https://doi.org/10.1016/j.buildenv.2011.01.032.

Schulte, N., Snyder, M., Isakov, V., Heist, D., Venkatram, A., 2014. Effects of solid barriers on dispersion of roadway emissions. Atmos. Environ. 97, 286–295. https://doi.org/10.1016/j.atmosenv.2014.08.026.

Setälä, H., Viippola, V., Rantalainen, A.L., Pennanen, A., Yli-Pelkonen, V., 2013. Does urban vegetation mitigate air pollution in northern conditions? Environ. Pollut. 183, 104–112. https://doi.org/10.1016/j.envpol.2012.11.010.

Steffens, J.T., Heist, D.K., Perry, S.G., Isakov, V., Baldauf, R.W., Zhang, K.M., 2014. Effects of roadway configurations on near-road air quality and the implications on roadway designs. Atmos. Environ. 94, 74–85. https://doi.org/10.1016/j.atmosenv.2014.05.015.

Steffens, J.T., Heist, D.K., Perry, S.G., Zhang, K.M., 2013. Modeling the effects of a solid barrier on pollutant dispersion under various atmospheric stability conditions. Atmos. Environ. 69, 76–85. https://doi.org/10.1016/j.atmosenv.2012.11.051.

Steffens, J.T., Wang, Y.J., Zhang, K.M., 2012. Exploration of effects of a vegetation barrier on particle size distributions in a near-road environment. Atmos. Environ. 50, 120–128. https://doi.org/10.1016/j.atmosenv.2011.12.051.

Tallis, M., Taylor, G., Sinnett, D., Freer-Smith, P., 2011. Estimating the removal of atmospheric particulate pollution by the urban tree canopy of London, under

current and future environments. Landsc. Urban Plan. 103, 129–138. https://doi.org/10.1016/j.landurbplan.2011.07.003.
Thaker, P., Gokhale, S., 2015. The impact of traffic-flow patterns on air quality in urban street canyons. Environ. Pollut. 208, 161–169. https://doi.org/10.1016/j.envpol.2015.09.004.
Tominaga, Y., Stathopoulos, T., 2013. CFD simulation of near-field pollutant dispersion in the urban environment: a review of current modeling techniques. Atmos. Environ. 79, 716–730. https://doi.org/10.1016/j.atmosenv.2013.07.028.
Tominaga, Y., Stathopoulos, T., 2009. Numerical simulation of dispersion around an isolated cubic building: comparison of various types of k − 3 models. Atmos. Environ. 43, 3200–3210. https://doi.org/10.1016/j.atmosenv.2009.03.038.
Tominaga, Y., Stathopoulos, T., 2007. Turbulent Schmidt numbers for CFD analysis with various types of flowfield. Atmos. Environ. 41, 8091–8099. https://doi.org/10.1016/j.atmosenv.2007.06.054.
Tong, Z., Baldauf, R.W., Isakov, V., Deshmukh, P., Max Zhang, K., 2016. Roadside vegetation barrier designs to mitigate near-road air pollution impacts. Sci. Total Environ. 541, 920–927. https://doi.org/10.1016/j.scitotenv.2015.09.067.
Venkatram, A., Snyder, M.G., Heist, D.K., Perry, S.G., Petersen, W.B., Isakov, V., 2013. Re-formulation of plume spread for near-surface dispersion. Atmos. Environ. 77, 846–855. https://doi.org/10.1016/j.atmosenv.2013.05.073.
Vos, P.E.J., Maiheu, B., Vankerkom, J., Janssen, S., 2013. Improving local air quality in cities: to tree or not to tree? Environ. Pollut. 183, 113–122. https://doi.org/10.1016/j.envpol.2012.10.021.
Wania, A., Bruse, M., Blond, N., Weber, C., 2012. Analysing the influence of different street vegetation on traffic-induced particle dispersion using microscale simulations. J. Environ. Manage 94, 91–101. https://doi.org/10.1016/j.jenvman.2011.06.036.
Wilson, J.D., 1985. Numerical studies of flow through a windbreak. J. Wind Eng. Ind. Aerodyn. 21, 119–154.
Xue, F., Li, X., 2017. Investigation on deposition effect of roadside trees on traffic released PM10 in street canyon. Sustain. Cities Soc. 30, 195–204. https://doi.org/10.1016/j.scs.2017.02.001.
Zauli Sajani, S., Trentini, A., Rovelli, S., Ricciardelli, I., Marchesi, S., MacCone, C., Bacco, D., Ferrari, S., Scotto, F., Zigola, C., Cattaneo, A., Cavallo, D.M., Lauriola, P., Poluzzi, V., Harrison, R.M., 2016. Is particulate air pollution at the front door a good proxy of residential exposure? Environ. Pollut. 213, 347–358. https://doi.org/10.1016/j.envpol.2016.02.033.